A cost-effective pH-sensitive release system for water source pH detection

Zhaoliang Zheng,[a,b] Xing Huang[c] and Dmitry Shchukin[b]

A facile and cost-effective strategy has been developed to form cobalt basic carbonate nanovalves at the orifice of mesoporous nanocontainers, which facilitates pH sensitive release of functional cargo for up-scaling towards application of water source pH detection.

Introducing the micro- or nano-level design into smart devices for feedback-controlled release has gained much more remarkable advancement in the fields of pharmacology and molecular biology than in others. The increasing concern about the well-being of human drove research in drug delivery or targeted therapy from fundamental to clinic.[1] On the contrary, the few successful examples to deliver fertilizer,[2] herbicide[3] and pesticide[4] in agriculture, corrosion inhibitor[5] and antifouling agent[6] in protective coating, and sensory material[7] in environmental detection, have only proved themselves in the lab. Particularly, environmental biologists found that fish eggs would not hatch in the water with pH lower than 5. The biodiversity also is gradually reduced as lakes and rivers become more acidic.[8] The widespread application of low-cost, stable and easy-to-handle pH sensitive detectors is urgently needed. However, the large gap between the conditions at research level and demands for large-scale applications appears because of the limits of existing manufacturing technologies and cost of raw materials.

Functionalized mesoporous materials have been adopted as an ideal platform for exploring novel approaches towards forming feedback release systems that can "survive" in much harsher conditions than in *vivo* environment. They provide a relatively stable porous structure and numerous selectable functionalizing agents, cargo molecules and strategies to seal the orifice. They are also potentially applicable in scaling-up production because it is convenient to find natural alternatives to synthetic materials, e.g. layered double oxides or halloysite nanotubes.[9] By now, however, we could not find any convincing work optimizing various important factors towards scaling-up production. Tarn *et al.*[10] designed a nanogate which can be latched shut simply by the strong chelate complex between two orifice-immobilized iminodiacetic acids and a cobalt ion. But the massive leakage of cargo would be inevitable if the process of closing the nanogate takes too long time, which decreases the effectiveness of the final product or even causes adverse impact due to premature exposure of the functional molecules. To minimize the premature release, Lvov's group has reported to form a stopper at the opening end of halloysites by means of quick complexation between loaded benzotriazole (BTA) and copper ions.[11] Closing the orifice took place in only one minute but was exclusively dependent on the specific BTA-Cu^{+} bonding,[12] which restricted the adaptability of such controlled release system in other applications. Supramolecular nanovalves based on pseudorotaxanes can regulate the release of a wide range of functional cargoes.[13] But the high cost of building blocks (e.g. price of cucurbit[7]uril hydrate = 1250 £/g, 545201 Aldrich) and complicated procedures to mechanize the silica nanocontainers always fail to realize their scaling-up production. Thus we can figure out the key factors that support a feedback controlled release system to be applicable in the fields other than pharmacology or molecular biology: simple procedure, low-cost raw material, high adaptability and effectiveness to control the release.

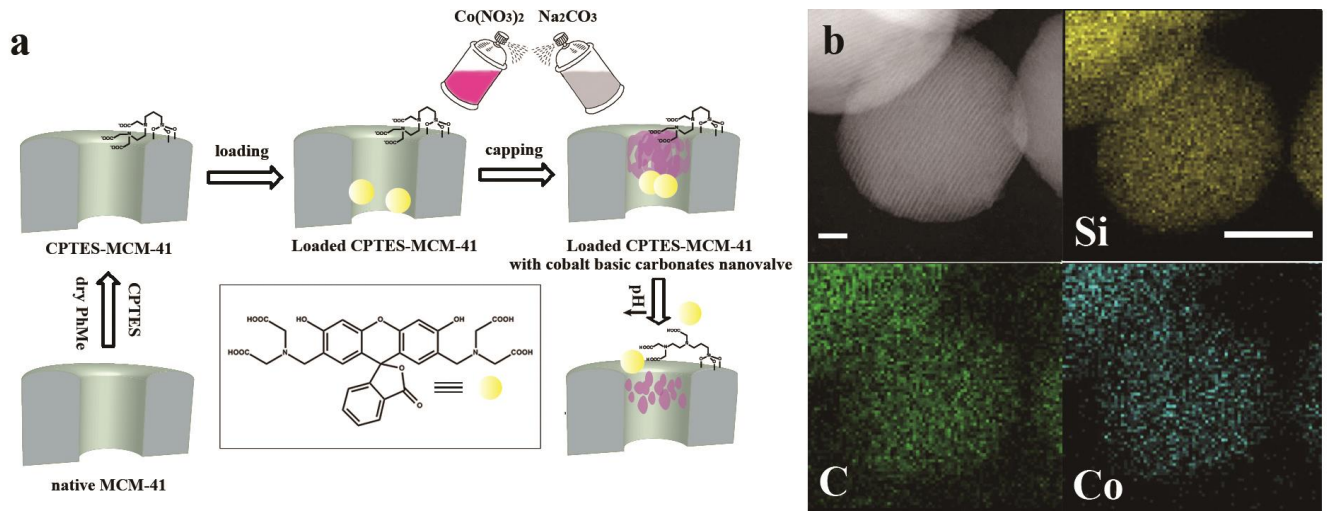

Fig. 1 (a) Schematic representation of preparation and operation of the acid responsive mechanized nanocontainers. (b) HAADF-STEM and elemental mapping images of loaded MCM-41 nanoparticle with nanovalves at its surface. Silicon, carbon and cobalt element mapping are presented. Scale bar: HAADF-STEM 50 nm, elemental mapping 100 nm.

In this communication, we report a facile and cost-effective strategy to form a pH-sensitive release system, which detains functional cargo within nanocontainers at neutral pH, and releases it in acidic environment at rate depending on the pH value. Fig. 1a shows a nanovalve system consisting of two components: 1. a three-dimensional (3D) porous cobalt basic carbonate nanoprecipitate formed by spraying $Co(NO_3)_2$ (0.1 M) and Na_2CO_3 (0.2 M) solutions on the loaded nanocontainers, and 2. ethylenediamine triacetate — an chelating agent that is immobilized at the orifice of silica MCM-41 nanoparticles via a one-step reaction, which serves as stabilizer for the nanovalves. Fig. 1b shows high angle annular dark-field scanning transmission electron microscopy (HAADF-STEM) images and elemental mapping of loaded MCM-41 nanoparticles with nanovalves at their surfaces. The Co mapping proves the distribution of the cobalt signal over the surface of the particles. Besides, the high contrast of carbon distribution between particle surface and carbon grid underneath confirms the presence of chelating agents and nanovalves. We compare the nanocontainers functionalized with ethylenediamine-triacetate, ethylenediamine-4-oxo-2-butenoic acid salt and diethylenetriamine moieties (Synthetic procedure and Table S1, ESI†). The organic content is intentionally tailored at around 0.2 mmol/g. Among three samples the ethylenediamine-triacetate-

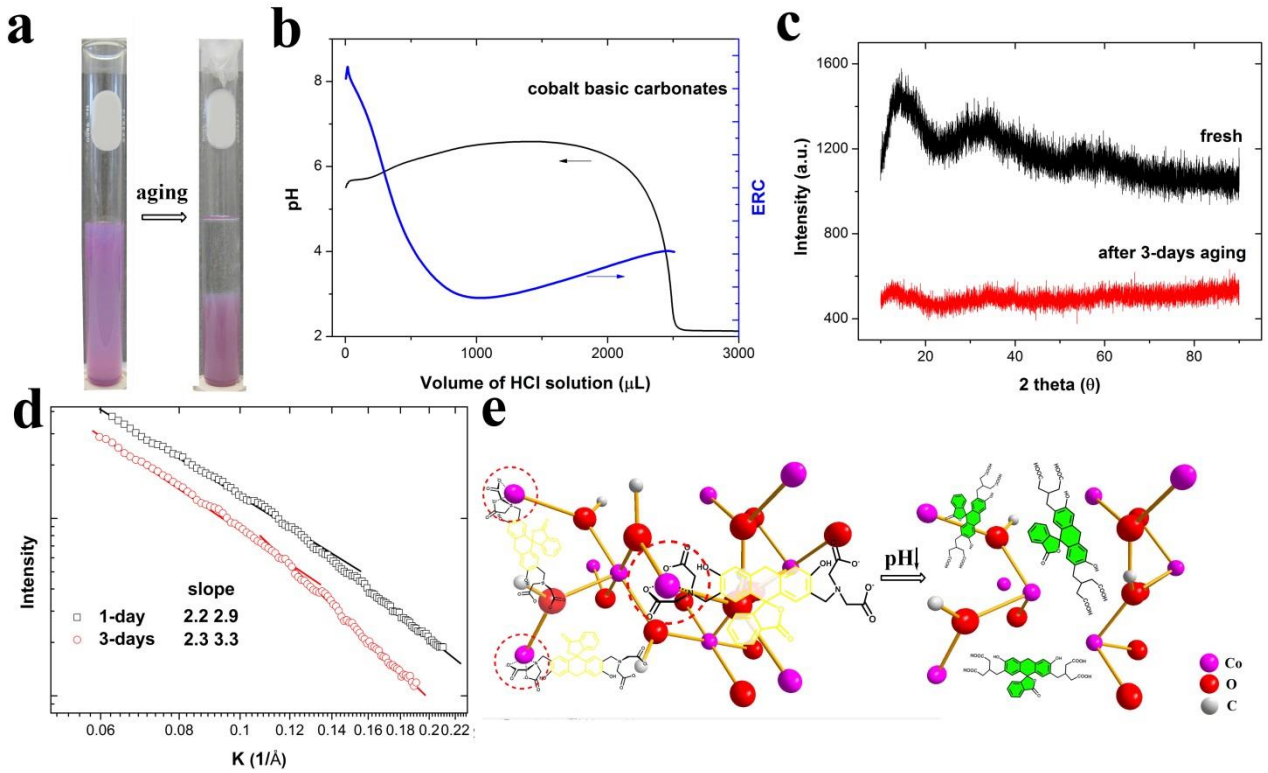

Fig. 2 (a) Comparison of cobalt basic carbonate precipitates between the beginning stage of flocculation and aging for three days under atmospheric pressure and in room temperature. (b) Titration and exothermic profile of cobalt basic carbonate precipitates. (c) XRD spectra of fresh cobalt basic carbonate precipitates and the ones after three-day aging. (d) Porod plots and corresponding slopes of 1- and 3-days aging at room temperature. (e) The two cartoons are modified from the crystal structure of $CoCO_3$ to highlight the chelating complexation between calcein and nanovalve, as well as acid induced partial and gradual dissolution of the valve structure and dissociation of Co^{2+}-calcein complex bonds. The cartoons also reveal that the detained calcein cargo emits weak fluorescence, but can yield strong green emission when it is released from the nanovalve.

functionalized nanocontainers exhibit the highest Co content at 1.7 wt%, as estimated by energy-dispersive X-ray spectroscopy (EDX), which is consistent with highest stability constant value of Co-ethylenediaminetetraacetate complex ($\lg K_{stab}$ = 16.21) over the one of Co-acetic acid (2.24) and Co-ethylenediamine (13.8).[14]

N_2 adsorption/desorption analysis demonstrates the one-step carboxylation of the silica nanocontainers, yielding a reasonably shrunken BET surface area of 791.9 m^2/g, pore diameter of 2.8 nm and pore volume of 0.63 m^3/g, respectively, as compared with native MCM-41 (Table S2, ESI†). The low content of carboxylate functionalization at 0.23 mmol/g (as determined by TGA) is undetectable with FTIR, but revealed by the negative ξ-potential (-45.3 ± 0.5 mV). Furthermore, the consumption of N-(trimethoxysilylpropyl)-ethylenediamine triacetic acid trisodium salt solution (CPTES, 45 wt% in water) is only 0.07 mL per gram of native MCM-41, which is much lower than in other works.[15] Small angle x-ray scattering (SAXS) revealed the regular mesoporous structure of MCM-41 nanocontainers is roughly preserved after the carboxylation and formation of nanovalves (Fig. S1, ESI†).

The cobalt basic carbonate nanovalve with 3D porous structure was formed by the quick complexation between divalent cobalt ions and the carbonate/hydroxide mixture.[16] Cobalt is an abundant metal resource on earth with production at 120,000 tons in 2013.[17] It is difficult to determine the porous structure of the nanovalve that is confined within the orifice of carboxylate-functionalized MCM-41. Their amorphous phase and unstable structure make it even difficult to directly detect the structure under high energy beam of microscopy technique. Thus we focused on the bulk gelatinous precipitates formed by quick reaction between $Co(NO_3)_2$ (0.1 M) and Na_2CO_3 (0.2 M) solutions (Fig. 2a left). The higher and lower concentrations of spraying solutions have also been considered (ESI†). The resulting magenta product maintained gel-like state after aging for three days, although almost 50% shrinkage in volume was detected (Fig. 2a right). The broad equivalence point recognition criteria (ERC) peak observed in the pH range of 6 to 2 in titration experiments indicates that the nanovalves contain a mixture of $CoCO_3$ and $Co(OH)_2$, which enables them to respond to pH lowering by gradual dissolution of the valve structure (Fig. 2b). Furthermore, the three-days-aged precipitates maintain a stable amorphous state without detectable crystallization, which can be confirmed by XRD (Fig. 2c). SAXS was also employed to confirm the 3D porous structure of the nanovalves. Fig. 2d reveals two successive power-law regimes at the Porod region[18] of the gelatinous precipitates after 3-days aging, with a mass fractal regime (d_f = 2.3) and a surface fractal regime (d_s = 2.7), because the slopes are 2.3 and 3.3, respectively. To track the structural evolution of the precipitate we record the SAXS pattern after 1-day aging (Fig. 2d), from which a dual-size distributed aggregate with smaller slopes can be already observed, indicating an intermediate state of 3D porous structure (ESI†). In our work, longer aging time (e.g. 10 days) will not further increase the slopes of the precipitates (Fig. S2), reflecting the structural stability of the nanovalves. The crossover occurs at K = 0.12 $Å^{-1}$, corresponding to a thickness of backbone, K^{-1} = 8.3 Å. Schaefer and Keefer[19] concluded such structure to be a 3D aggregate with rough pores and fractal backbones. The highly porous structure and the thinnest backbones of cobalt basic carbonates ever reported[15] can be ascribed to the amorphous phase derived from the rapid complexation process.[20] In addition, the radius of gyration of the nanovalve is predicted to be around 22 Å by measuring the Guinier radius of the initial curvature of the SAXS curve[21] (Fig. S3, ESI†), which matches the pore diameter of the functionalized silica orifice. It is also noteworthy that a relatively large surface area (75.28 m^2/g) of bulk cobalt basic carbonates is preserved from coarsening by the 3D porous structure, which is in agreement with the observation in Fig. 2a. Therefore, it is reasonable to adopt the cobalt basic carbonates as a nanovalve due to their stable and porous structure, suitable size matching the diameter of mesopores, easiness of fabrication and low cost of raw material.

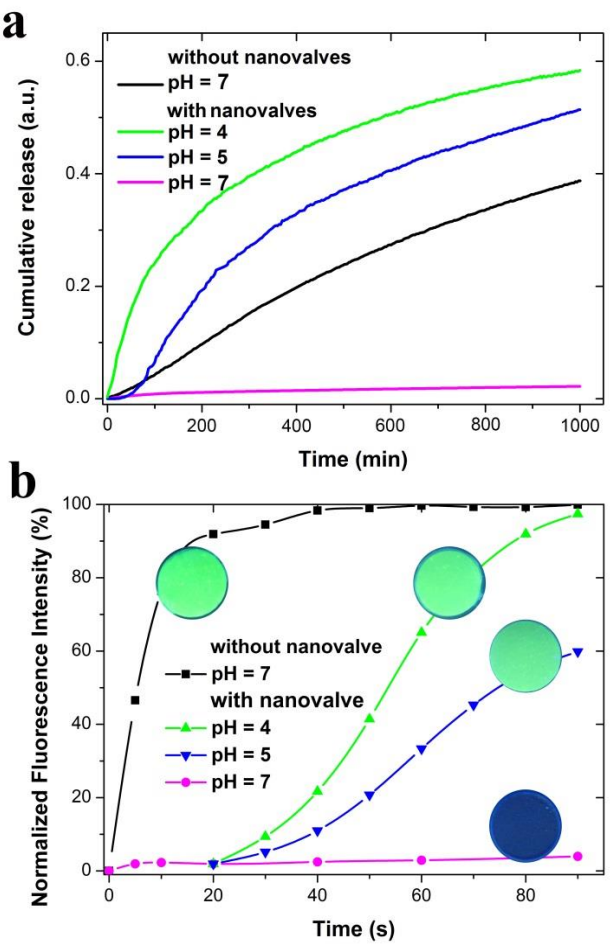

Fig. 3 (a) Release profile of calcein from loaded nanocontainers with Co-Carbonate nanovalves. (b) Fluorescence intensity of tablets as a function of time. The intensity was analysed with Leica's fluorescence software and normalized with the equilibrium intensity of the sample with uncapped calcein-loaded nanocaontainers. The inset image (1) implies that the loaded containers with Co-Carbonate nanovalves exhibit no emission in neutral pH. But the green fluorescence can be observed within 60 s at pH = 5 (2) and 10 s at pH = 4 (3) . The inset image (1) represents the tablet containing calcein loaded containers without Co-Carbonate nanovalves, which exhibits green fluorescence immediately after immersion in water with neutral pH. The diameter of the tablets is about 10 mm.

Calcein was selected for pH detection as the model cargo molecule in our work due to its chemical and optical properties. First, the aggregated calcein emits weak fluorescence when confined within the mesopores, but the diffused one into the bulk aqueous solutions can yield strong fluorescence emission, which allows reducing the cargo loading. Second, the fluorescence emission of calcein is almost independent from pH change.[22] Third, Fig. 2e highlights that Co^{2+} can form a stable complex with single iminodiacetic acid end group with a stability constant ($\lg K_{stab}$) at around 7[23] but with a pair at 16.21, which helps detain the cargo by the cobalt basic carbonate nanovalve. At the same time, the 3D porous nanovalve provides a

large number of unsheltered Co^{2+} centers due to the amorphous state and the relatively large surface area, which also facilitates the strong chelating complexation. Such complex bonds usually deform in response to a pH lowering due to the protonation of electron donating agents[10, 12]. Thus, the controlled release system that is sensitive to acidity of bulk solution can be constructed with inherent pH-sensitivity of the cobalt basic carbonate nanovalve and complex bonds (Fig. 2e, right panel). The 3D porous nanovalves that detain the calcein molecules with chelating complexation will be partially and gradually dissolved as the pH value decreases. At the same time, the pH sensitive chelating complexation will also be dissociated due to the protonation of complex agents. Although the loaded calcein molecules in aggregation state emit a weak fluorescence, they can yield a strong fluorescence emission in bulk aqueous solution when the nanovalves are opened.

Fig. 3a shows the pH-sensitive release of calcein cargo. Comparing with the release profile without nanovalves at neutral environment, the flat baseline confirms the effective detaining effect offered by the nanovalve and thus the negligible premature leakage of calcein. It indicates that the nanovalve can keep up calcein for a long serving time in neutral condition and release it as a feedback to the external trigger when necessary. The lag phase at the initial stage of release at pH = 5 indicates a slow process of dissolving nanovalves in such a weak acidic environment. A burst release of the dye without any waiting time can be obtained when the surrounding medium is further acidified to pH = 4. The notable difference in response to pH value may help us detect the pH of polluted water sources in a rapid and direct way. Furthermore, we checked the influence of ionic strength, concentration of transition metal ions and chelating anions (ethylenediaminetetraacetic acid (EDTA)) on the pH sensitivity. As shown in Fig. S4, the premature leakage of loading calcein in neutral becomes obvious when the concentration of $NaNO_3$ is increased to 0.2 mol/L. The release of cargo molecules is further accelerated in acidic condition with high ionic strength. The fluorescence spectroscopy can detect the pH-sensitive release at pH = 5 when the concentrations of transition metal ions (Cu^{2+}, Zn^{2+}, Fe^{2+} and Mn^{2+}) are below 0.5 mg/L (Fig. S4). The higher concentrations will induce invalidation because of the fluorescence quenching induced by chelating complexation. The effect of anions on the pH sensitivity has also been examined. Our pH-responsive system can resist the concentration of EDTA up to 1500 ppb which is slightly higher than the safe upper-limit of the river (1120 ppb) in England[24]. Thus our pH-responsive system may have promising application for detecting some hazard anions. The nanovalve can also control the release of other cargo that forms a strong complex with divalent cobalt ions. For example, benzotriazole that forms a stable complex with Co^{2+} can also be released from the nanocontainers in response to pH change (Fig. S5, ESI†). The resulting controlled release system has potential application in self-healing anticorrosion coating.

As a step towards achieving our goal of scaling up the fabrication of containers with cobalt basic carbonate nanovalves for environment detection, we pressed the mixture of aluminum oxides and calcein-loaded containers with or without Co-Carbonate nanovalves into tablets (Fig. S6, ESI†) for pH detection. Inset image (1) in Fig. 3b reveals that the tablet containing capped nanocontainers is colorless in neutral condition but exhibits a green emission in acidic environment. The color can be visibly detected within 1 min at pH = 5 and within only 10 s at pH = 4 (inset image (2) and (3), respectively). The notable difference in pH responsive green fluorescence can help directly and quickly distinguish the pH value of the water resource. On the contrary, the uncapped nanocontainers release calcein immediately after their immersion in water at neutral pH (inset image (4)). In addition, the fluorescence intensity at the edge part of the tablets was also recorded. Fig. 3b reveals that the tablet with capped nanocontainers emits very weak fluorescence after immersion in neutral condition for 20 s. Once it was moved to the environment with pH = 5, the intensity increases gradually with time. During the same period, the nanovalve structure would be further dissolved in pH = 4, which results in a quicker release of calcein and the fluorescence intensity reaches a saturate level within only 90 s. A sharp rise of the fluorescence intensity can be found for the sample containing uncapped loaded nanocontainers, implying the importance of the cobalt basic carbonate nanovalves in reserving cargo in neutral environment. Using the easy-handling product, we can also detect our working and living environment condition. The tablets exhibit invisible green emission after 20 s immersion in the water samples collected from university campus and residential area near a food factory (Fig. S7, ESI†), implying a safe outdoor environmental quality for people to enjoy their working and living. The pH values of wild water samples were then confirmed by a pH meter, with 7.4 in university campus and 7.0 near the food factory.

In summary, we demonstrated a facile and cost-effective way to fabricate a pH-sensitive release nanovalve system that has the advantages of simple procedure, low-cost raw material, high adaptability and effectiveness to control the release. The cobalt basic carbonate nanovalves exhibit effective control over cargo storage and release at different pH range. The proposed nanovalves can be easily up-scaled to the substantial quantities for their implementation in the fields requiring storage and controlled release in the condition other than vivo environment.

We thank Ingrid Zenke at the Max Planck Institute of Colloids and Interfaces for SAXS measurement. This work was financially supported by EU FP7 Byefouling and FP7 NanoBarrier project of the EU Commission. We also thank the support by the Brian Mercer Feasibility Award from Royal Society of Chemistry, UK.

Notes and references

[a] Max-Planck Institute of Colloids and Interfaces, 14424, Potsdam, Germany

[b] Stephenson Institute for Renewable Energy Department of Chemistry, University of Liverpool, Crown Street, Liverpool, L69 7ZD, UK.

[c] Fritz-Haber-Institut der MPG, Faradayweg 4-6, 14195, Berlin, Germany.

† Electronic Supplementary Information (ESI) available: [details of any supplementary information available should be included here]. See DOI: 10.1039/c000000x/

1 C. Alvarez-Lorenzo and A. Concheiro, *Chem. Comm.*, 2014, **50**, 7743.

2 A. Bortolin, F. A. Aouada, M. R. de Moura, C. Ribeiro, E. Longo and L. H. C. Mattoso, *J. Appl. Polym. Sci.*, 2012, **123**, 2291.

3 X. J. Wang and J. Zhao, *J. Agric. Food Chem.*, 2013, **61**, 3789.

4 Y. B. Xiang, N. Wang, J. M. Song, D. Q. Cai and Z. Y. Wu, *J. Agric. Food Chem.*, 2013, **61**, 5215.

5 J. J. Fu, T. Chen, M. D. Wang, N. W. Yang, S. N. Li, Y. Wang and X. D. Liu, *Acs Nano*, 2013, **7**, 11397.

6 C. Zhao, L. Y. Li, Q. M. Wang, J. Zhao, X. Yu and J. Zheng, *Abstr. Pap. Am. Chem. S.*, 2012, **243**; Y. Le, P. T. Hou, J. X. Wang and J. F. Chen, *Mater. Chem. Phys.*, 2010, **120**, 351.

7 D. M. Liu, K. D. Lu, C. Poon and W. B. Lin, *Inorg. Chem.*, 2014, **53**, 1916.

8 H.-W. Gao and X.-H. Xu, *Chem. Comm.*, 2011, **48**, 12810; H.-C. Teien, W. J. F. Standring, B. Salbu, M. Marskar, F. Kroglund and A. Hindar, *J. Environ. Monitor.*, 2004, **6**, 191.

9 E. Abdullayev, V. Abbasov, A. Tursunbayeva, V. Portnov, H. Ibrahimov, G. Mukhtarova and Y. Lvov, *ACS Appl. Mater. Interfaces*, 2013, **5**, 4464.

10 D. Tarn, M. Xue and J. I. Zink, *Inorg. Chem.*, 2013, **52**, 2044.

11 E. Abdullayev and Y. Lvov, *J. Mater. Chem.*, 2010, **20**, 6681.

12 Y. Li, M. L. Gong, K. Ramji and Y. Z. Li, *J. Phys. Chem. C*, 2009, **113**, 18003.

13 M. Li, H. Yan, C. Teh, V. Korzh and Y. Zhao, *Chem. Comm.*, 2014; T. Chen, N. W. Yang and J. J. Fu, *Chem. Comm.*, 2013, **49**, 6555; N. M. Khashab, M. E. Belowich, A. Trabolsi, D. C. Friedman, C. Valente, Y. N. Lau, H. A. Khatib, J. I. Zink and J. F. Stoddart, *Chem. Comm.*, 2009, 5371; M. W. Ambrogio, C. R. Thomas, Y.-L. Zhao, J. I. Zink and J. F. Stoddart, *Accounts Chem. Res.*, 2011, **44**, 903.

14 T. E. Furia, Chap. 6, *CRC Handbook of Food Additives, Second Edition*, Taylor & Francis, 1980.

15 D. He, X. He, K. Wang, Y. Zhao and Z. Zou, *Langmuir*, 2013, **29**, 5896.

16 R. Xu and H. C. Zeng, *The J. Phys. Chem. B*, 2003, **107**, 12643.

17 *Commodity Statistics and Information*, *http://minerals.usgs.gov/minerals/pubs/commodity/cobalt/mcs-2014-cobal.pdf*.

18 D. W. Schaefer, A. J. Hurd, D. K. Christen, S. Spooner and J. S. Lin, *MRS Online Proceedings Library*, 1988, **121**, null.

19 D. W. Schaefer and K. D. Keefer, *Phys. Rev. Lett.*, 1986, **56**, 2199.

20 W. D. Kingery, H. K. Bowen and D. R. Uhlmann, *Introduction to ceramics*, Wiley, 1976.

21 C. J. Brinker, K. D. Keefer, D. W. Schaefer and C. S. Ashley, *J. Non-Cryst. Solids*, 1982, **48**, 47.

22 J. S. Liu and X. Z. Du, *J. Mater. Chem.*, 2010, **20**, 3642.

23 G. Schwarzenbach, G. Anderegg, W. Schneider and H. Senn, *Helv. Chim. Acta*, 1955, **38**, 1147.

24 EDTA environment safety standards. Available online: http://www.epa.gov/opprd001/inerts/edta.pdf